

**DIAMOND FORTUNE Seismic Acceleration Measurements
H. D. Garbin
Experimental Design/Analysis & Computing Support Department
Sandia National Laboratories
Albuquerque, New Mexico 87185-1169**

ABSTRACT

DIAMOND FORTUNE was a nuclear explosion detonated inside an 11 m hemispherical cavity in tuff at the Nevada Test Site. Previous cavity explosions such as STERLING and MILL YARD have shown a substantial decrease in the expected ground motion. These types of cavity tests present a serious problem for a Comprehensive Test Ban (CTB). Not only is detection a problem, but presently there is no seismic method to discriminate between a tamped and cavity explosion. DIAMOND FORTUNE allowed us to examine several aspects of a cavity explosion in the context of a CTB. On this test, there were two groups of accelerometers fielded. One group was located in the free-field at sites above and below the cavity within 30 m of the source. The second group consisted of a line of gauges placed in the invert of P-tunnel extending from 44 m to 224 m from the source. The purpose of this arrangement was to measure ground motion in an effort to detect a non-symmetric radiation pattern due to the hemisphere, examine the high frequency propagation of the free-field signals as a possible discriminate, and calculate the decoupling factor.

The radiation pattern experiment was conducted in an effort to determine if the asymmetry of a hemispherical cavity could provide a preferred direction of transmission. The analysis indicated a definite radiation pattern with larger amplitudes transmitted through the spherical surface than the plane surface. The high frequency discrimination experiment used the gauges located in the tunnel invert. The possibility of using high frequency signals as a discriminant of tamped versus cavity explosions is implied by the MILL YARD data. MILL YARD was also a nuclear explosion in an 11 m hemispherical cavity. The free-field ground motion signals from this test (<25 m) contained very large high frequency amplitudes (≈ 1000 Hz) in their spectra. DIAMOND FORTUNE also exhibited high frequency signals with corner frequencies twice that of the scaled tamped DISTANT ZENITH event. These corner frequencies varied from 500 Hz within 30 m of the source to 70 Hz at the outer most range of 224 m. The low frequency decoupling factor could not be determined due to some difficulties with low frequency noise and the length of the scaled time window of the reference event. However, for frequencies above 10 Hz, DIAMOND FORTUNE had a decoupling factor between 10 and 30.

Acknowledgments

I wish to thank all the people associated with making the free-field experiment a success. The gauges were built by Cliff Kinabrew and Sonny Peppers fielded the gauges and interacted with the recording people. The recording was accomplished with Departments 9321, 9323 and 9324. Gary Miller, Mike Burke and Jerry Chael provided invaluable service at NTS interacting with tunnel personnel. Al Chabai provided continued support throughout the project with valuable discussions. Eric Chael and Tom Bergstresser reviewed the report and offered valuable comments.

Introduction

Understanding the phenomenology of cavity explosions is important to both nuclear treaty verification and nonproliferation. The detonation of a nuclear explosion in a large air-filled cavity is a serious evasion scenario that a Comprehensive Test Ban Treaty (CTBT) must address. It has been known for decades that seismic signals emanating from such an explosion are muffled as much as two orders of magnitude. This was demonstrated in salt by the SALMON and STERLING¹ events and in tuff by MILL YARD². STERLING was detonated in the 17 m spherical cavity produced by the SALMON event and MILL YARD was conducted in an 11 m hemispherical cavity mined in tuff. Both of these events had decoupling factors near or greater than 70 which could allow a nuclear test to remain undetected at regional ranges. To further our understanding of decoupling, it is advantageous to make measurements on other cavity events to verify previous results and further investigate other aspects of cavity decoupling.

DIAMOND FORTUNE was a small nuclear event conducted in P-tunnel on April 30, 1992 in an 11 m radius hemispherical cavity. This event provided us with opportunities for obtaining data relevant to verification. As in other studies, decoupling analysis requires a reference event for comparison with the cavity event. In this study, DISTANT ZENITH is used as the reference event since it was a normal tamped test with a known yield also in P-tunnel within 1 km of DIAMOND FORTUNE. Ideally, if a dedicated decoupling test was to be conducted, the reference test would consist of a tamped source of known yield with the ground motion measured at various ranges. A second test then would be conducted in the cavity formed where the tamped source was located with the same yield and the ground motion measured by the same gauges located at the same ranges. Normally nuclear tests are not conducted in this manner and the reference events are tamped tests with different yields and with gauges at different ranges than the cavity event. To adjust for these differences, the reference event is cube root scaled to the yield of the decoupled event (DIAMOND FORTUNE) and corrections are made for the range. Besides allowing measurement of decoupling, the configuration of the cavity (hemispherical) also offers us the chance to investigate variations in the seismic radiation pattern. The spherical geometry of the STERLING event simplified the analysis and interpretation considerably. Although MILL YARD occurred in a hemispherical cavity, there was no attempt to measure the effect of the geometry on the seismic radiation pattern. By examining the seismic signals transmitted from the cavity in a non-symmetric plane, we can see if the energy can be enhanced or weakened in predictable directions. The design of a cavity geometry could make the source more earthquake-like or perhaps focus signals away from known seismic nets. Note that DIAMOND FORTUNE was considered a fully decoupled test and perhaps a more relevant experiment would consist of a test in an overdriven cavity.

The above discussion of decoupling and non-symmetric radiation pattern illustrate that decoupling is a viable evasion technique. From the seismic point of view, the advantage appears to be with the evader since presently there is no seismic method of distinguishing a tamped explosion from a cavity explosion. DIAMOND FORTUNE allows us to investigate possible discriminates to defeat this decoupling scenario. One possible near-field cavity discriminant is suggested by the MILL YARD event. MILL YARD was almost seismically identical to the DIAMOND FORTUNE test. Free-field signals measured on MILL YARD had very high frequency components (1000 Hz) in the time series. The gauges were accelerometers placed very close to the device at 17 and 24 m ranges from Surface Ground Zero (SGZ) of the cavity. If these high frequency signals are propagated out to ranges of several hundred meters, they could be a possible discriminant between a tamped and cavity event in an On Site Inspection (OSI) context. The DIAMOND FORTUNE experiment adds to our understanding of detection and discrimination of cavity explosions, exhibit the possible

directionality of seismic energy produced by a non-spherical symmetric source, and verify the amount of decoupling associated with a cavity event.

Description

The DIAMOND FORTUNE seismic experiment had two distinct parts designed to examine two different phenomena; the asymmetric emission of energy from the source and the near-field high frequency propagation from the source. The radiation pattern experiment was instrumented by locating, at different heights around SGZ of the cavity, four two-component accelerometers packages. The gauges were installed in two 6' boreholes drilled in a symmetrical manner above and below the cavity. Two of these sites were located almost directly above and below SGZ. The other two were at 45° above and below the SGZ horizon. Figure 1 depicts the experimental layout with respect to the cavity. Each instrument package had two systems associated with it, one to monitor the high frequency (hf) signals and the other the low frequency (lf) signals. The hf system consisted of a two-component 1000 g gauges sampling at 100 kHz. In spherical coordinates with the origin at the hemisphere center (SGZ), the components were aligned radially and along the polar angle. In this configuration, the radial component points to the cavity SGZ and the polar component is tangential to the sphere pointing towards the vertical axis of the hemisphere. Any twisting of this plane of the accelerometer components was controlled by a level during installation and the alignment of the gauges is within 5°. In each case, the total recording time was 0.08 sec. The lf system consists of a similar arrangement but with 100 g gauges and a sample rate of 10 kHz. Its total recording time was 0.8 sec.

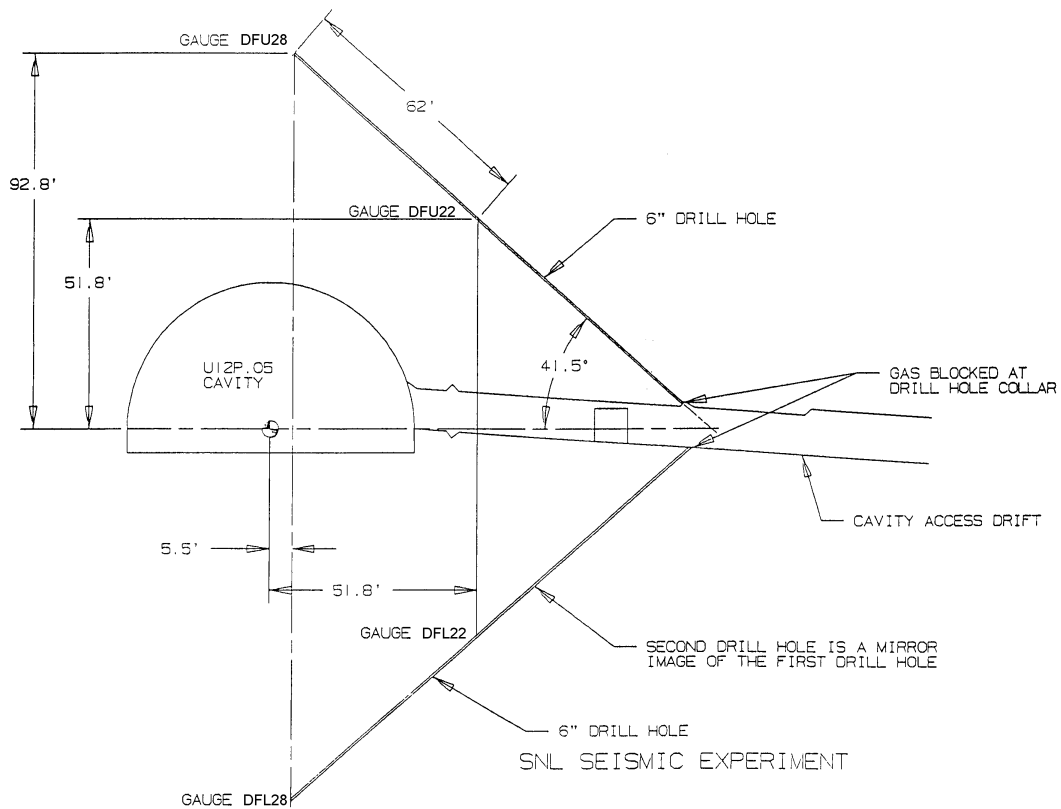


Figure 1

Side View of DIAMOND FORTUNE Radiation Experiment

To monitor the high frequency propagation of the signals, a line of seven single axis radial accelerometers was installed and arranged in as linear an array as the tunnel configuration would allow. The gauges were put in 10 m boreholes in the invert of P tunnel as shown in figure 2. The boreholes are located at ranges from 44 to 224 m in 30 m intervals. The array has a radial spread from SGZ of about 30°. The signals were sampled at 10 kHz.

Figure 2

High Frequency Acceleration Experiment

Predictions:

Estimates of the peak accelerations at all the sites were made prior to the test. The standard method uses empirical curves relating scaled peak amplitude to scaled range similar to those developed by Perret and Bass³. This is not appropriate here because the test was fully decoupled and the Bass curves are relevant to tamped events. However some free-field data was measured on the MILL YARD event² and are used to fix an upper bound on the peak amplitudes. These MILL YARD gauges were located at ranges of 17 and 24 m which directly give a good amplitude estimate for accelerations located near the cavity. The yields of MILL YARD and DIAMOND FORTUNE are assumed to be the same so no scaling is required. The DIAMOND FORTUNE amplitudes at the more distant ranges are estimated by propagating the MILL YARD free-field signals out to the appropriate distance. This is accomplished by using the MILL YARD signals as a driving function to calculate estimated ground motion at greater ranges. Let the MILL YARD signal be given as $u(t)$. The Fourier Transform of the signal is:

$$u(\omega) = \int_{-\infty}^{\infty} u(t)e^{-\omega t} dt \quad (1)$$

where t -time
 ω -angular frequency.

A compressional wave can be expressed as:

$$u(\omega) = \frac{\partial \Phi(\omega)}{\partial r} \quad (2)$$

where Φ is the Reduced Displacement Potential (RDP) and r is the range.

Φ satisfies the spherical wave equation and it can be shown to be

$$\Phi(\omega) = A(\omega)e^{ikr} / r \quad (3)$$

$A(\omega)$ depends on the boundary conditions and k is the wave number (ω/α) and α is the compressional wave velocity.

Thus, from the expressions (2) and (3), the ground motion can be expressed as:

$$u(\omega) = A(\omega) \left\{ \frac{ik}{r} - \frac{1}{r^2} \right\} e^{ikr} \quad (4)$$

To propagate the wave from r_1 to r_2 , form from expression (4) the ratio:

$$u_2(\omega) = u_1(\omega) \frac{(ikr_2 - 1) \left(\frac{r_1}{r_2} \right)^2}{(ikr_1 - 1)} e^{ik(r_2 - r_1) - k(r_2 - r_1)/2Q} \quad (5)$$

Attenuation has been added in equation (5) through the quality factor Q . This expression is used to estimate the ground motion of DIAMOND FORTUNE. $u_1(\omega)$ is the free-field MILL YARD data. The time series at the new range, r_2 , is calculated from the Inverse Fourier Transform of $u_2(\omega)$. Q is either assumed or estimated from previous tests. A Q factor of 50 was used which was much too high and gave a conservative estimate of the peak amplitudes. This insured that the band edges would be set high so clipping would not be a problem at the expense of lower signal to noise. A more realistic value of Q is 10 to 15.

Results

1) Radiation Pattern

Representative plots of the data are shown in figures 3 - 5 below. Figure 3 shows the radial accelerations of the gauges located above SGZ and figure 4 shows the corresponding signals below the cavity. The amplitudes are much larger on the gauges located above SGZ with peaks of 91 g directly above (source range = 27.3 m) and 230 g at 45° (source range = 18.4 m). The corresponding peaks beneath SGZ are much lower, 15 g and 18 g directly below SGZ (range = 34.0 m) and at 45° (range = 25.9 m) respectively. Some of the amplitude differences between the upper and lower gauges are caused by attenuation in the greater path distances traveled through the tuff by the rays below the cavity. The transmission coefficients of the spherical and plane surfaces also have an effect. An elastic calculation is done later to quantify these energy losses. Figure 5 is a plot of the two orthogonal components for the gauges above the cavity at 45°. The lower plot in the figure is the

radial component offset by 0.01 sec. Note that the polar component (upper curve) has a large amplitude of 100 g or 40% of the radial signal. This percentage holds generally for all the sites except the instruments located directly below SGZ. The magnitude of the polar amplitude is probably due to the asymmetry in the hemispherical shape of the cavity coupled with the off-center location of the source causing the rays to be refracted from the radial direction.

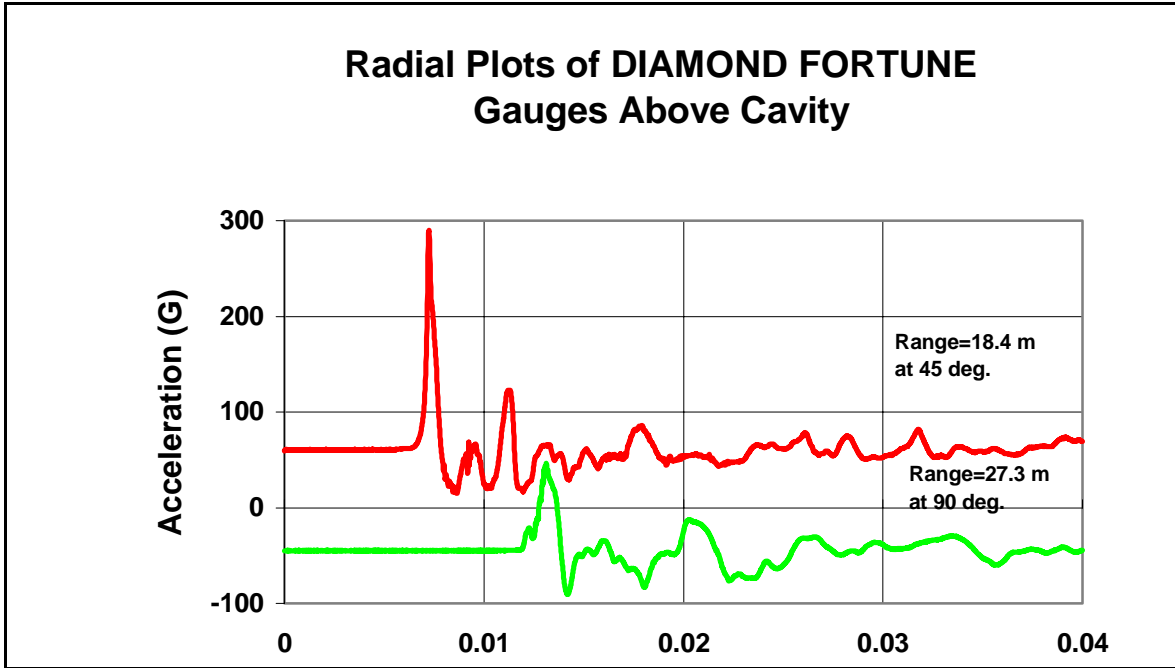


Figure 3

Radial Signals Above the Cavity

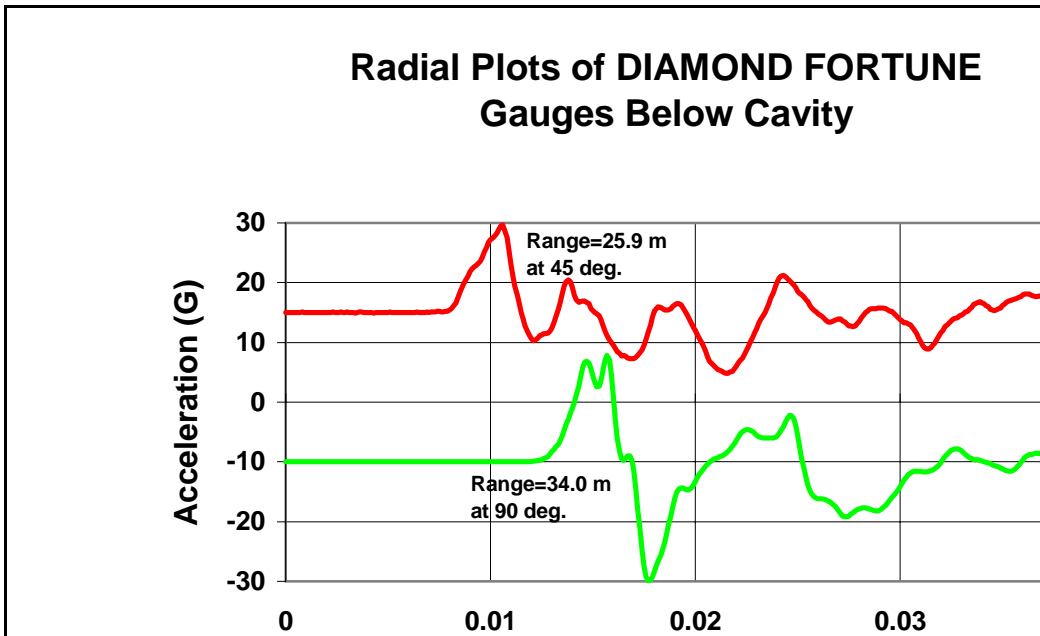


Figure 4

Radial Signals Below the Cavity

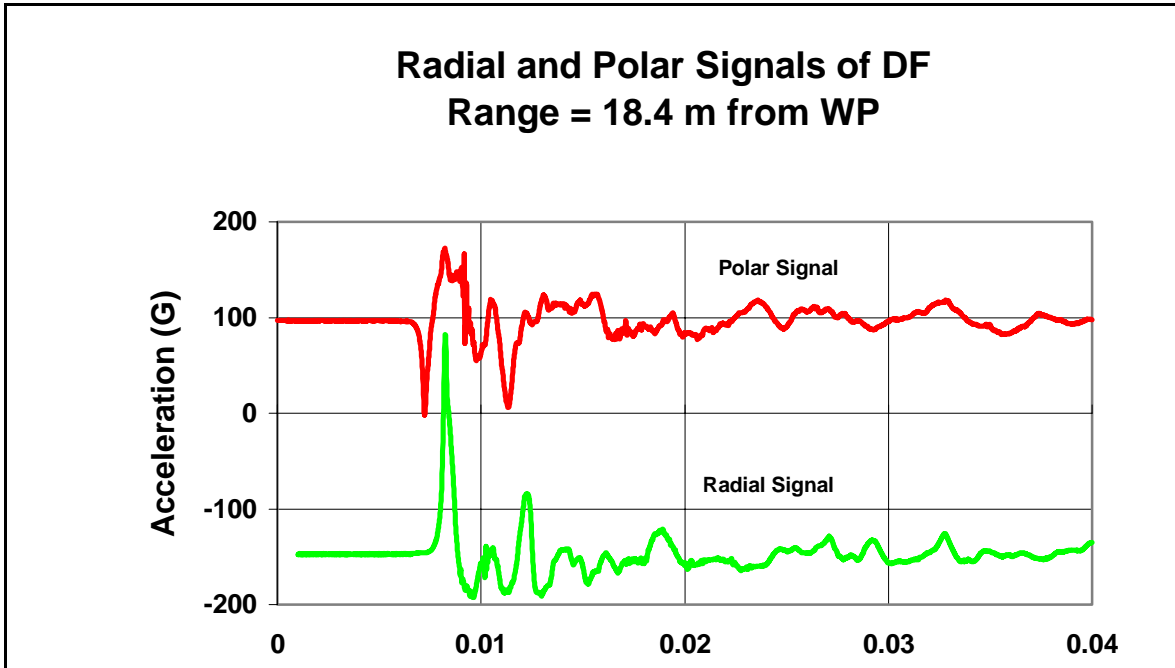


Figure 5

Orthogonal Components Above Cavity at 45°

Table I lists completely the initial peaks for each channel beginning at the site directly over SGZ. The station identifier is DF for DIAMOND FORTUNE, U or L for upper or lower locations with respect to the cavity, 22 or 28 is the approximate slant range in meters to SGZ, and R or P specifies either the radial or polar component. The ranges listed in the table are the actual ranges from the source to the gauges. This table reiterates the conclusions drawn from the plots: There are larger radial peak accelerations above the cavity than below. The table also shows there is significant non-radial motion at all locations except directly below SGZ, where its polar component as represented by DFL28P is small compared to its radial peak (DFL28R). This is not unexpected due to the interaction of the wave with a plane surface. In this case, there is little mode conversion or refraction because the ray path runs almost normal to the planar floor of the hemisphere.

Table of Peak Radial Signals

	Range (M)	Peak Acc. (G)
DFU28R	27.3	91.4
DFU28P	27.3	35.0
DFU22R	18.4	230.0
DFU22P	18.4	100.0
DFL22R	25.9	14.6
DFL22P	25.9	6.1
DFL28R	34.0	17.8
DFL28P	34.0	1.2

Table I

Peak Accelerations for Gauges in Radiation Experiment

To examine whether energy is transmitted more favorably in certain directions, I compared low frequency signals at the different azimuths. Low frequencies are used because the ground acts like a low pass filter and this is the part of the spectrum that is transmitted to the far-field. Figure 6 is a plot of the radial signals of each site which are low pass filtered at 25 Hz. The signal identifiers are the same as described earlier. A low pass filter with a corner frequency of 25 Hz is chosen because it has been shown that at this frequency the spectra of NTS explosions at regional ranges merge into the noise⁴. The two topmost plots are data for the gauges at 45° and the two lower plots are the responses on the vertical above and below the cavity. The 25 Hz is specific to NTS and higher frequencies are detectable at the regional ranges from other test sites⁵.

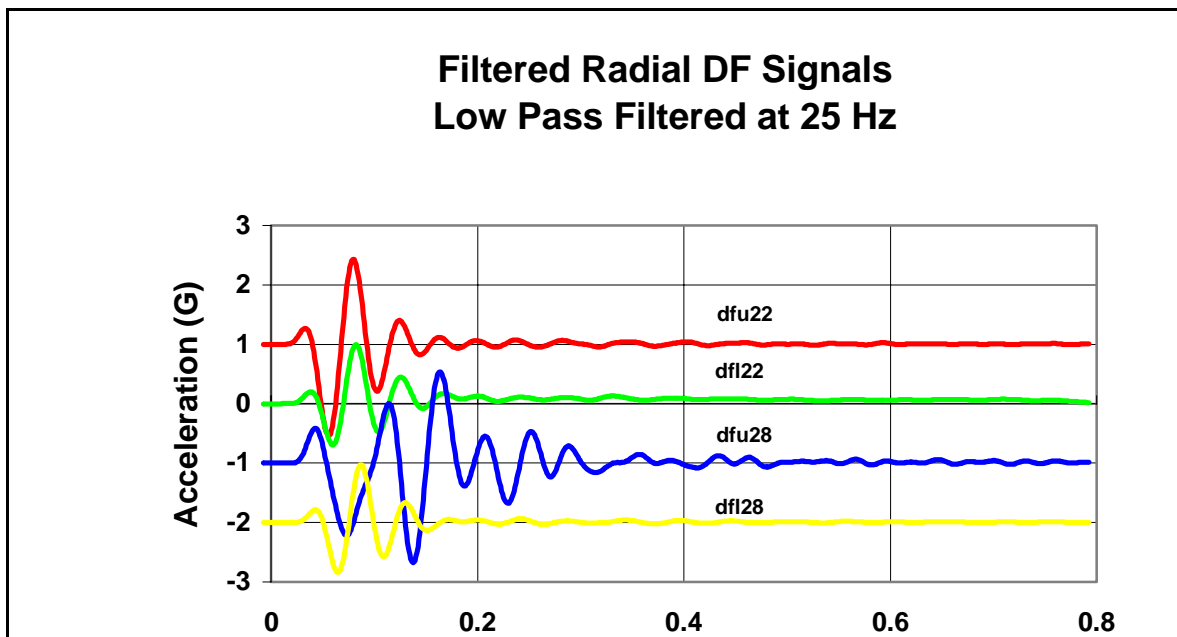


Figure 6

Radial Acceleration Data Low Pass Filtered at 25 Hz

	p (G)	p-p (G)
DFU22	0.27	1.53
DFL22	0.20	0.69
DFU28	0.59	1.22
DFL28	0.22	0.84

Table II

Peak Amplitudes of Filtered Signals (LP 25 Hz)

Table II is a list of the first peak and next peak to peak amplitudes of the signals in figure 6. These peaks indicate a degradation of the signal that is propagated downward into the plane surface on the floor. The average peak ratios between the companion gauges (above and below GZ) is about 2. Part of this decrease in signal strength can be explained by the different ranges traveled upward and downward to the gauges. The ranges as listed in table I show DFU28 closer to the device than DFL28. However the geometric spreading correction is only a factor of 1.2. Attenuation is not a major factor of signal decay since the wavelength of a 25 Hz signal in tuff is over 100 m, a mere fraction of the range differences between gauge locations. This is not true for the high frequency signals and the attenuation in tuff must be included. Finally, there is an additional factor in the paths of the signals which can cause signal loss. The transmission through a spherical surface is different than the transmission through a plane surface. I made elastic calculations of transmission coefficients of these geometries in an attempt to reproduce the peak amplitudes of the unfiltered data for the gauges directly above and below GZ. This is the simplest case since the rays are almost normal to each surface and avoid mode conversion and refraction effects. The analysis is based on the linear wave equations with an interaction of a spherical wave on a spherical surface and a spherical wave on a plane surface. To facilitate the spherical surface calculation, the source is assumed to be at the center of a sphere. Although this is not true since the source is elevated above ground zero, it is a first approximation for the signal propagating up the vertical axis. The symmetric calculation of a spherical wave and a spherical interface can be done exactly and the boundary conditions give the transmission coefficient T_s :

$$T_s = \frac{2ix_a^3(ix_1 - 1)}{\left[x_a^2(ix_1 - 1) - \frac{\mu}{\kappa}(ix_a + 1)(-3x_1^2 - 4x_1i + 4) \right](ix_a - 1)} \quad (6)$$

where $x_1 = \omega a / v$
 $x_a = \omega a / c$
 μ = shear modulus of medium
 κ = bulk modulus of air
 v = p-wave velocity in medium
 c = shock velocity in air
 a = cavity radius
 ω = circular frequency = $2\pi \cdot \text{freq.}$

The other transmission coefficient deals with a spherical wave impinging on a plane surface. The simplest solution has the gauge directly below the source and this is the problem solved. A solution

is found by assuming image sources for both the reflected and refracted waves and satisfying the boundary conditions on the plane surface. The result of this calculation gives the transmission coefficient T_p :

$$T_p = \frac{2ix_2^3(ix_3 - 1)}{\left[x_2^2(ix_3 - 1) - \frac{\mu}{\kappa}(ix_2 + 1)\frac{v}{c}(-3x_3^2 - 4x_3i + 4) \right](ix_2 - 1)} \quad (7)$$

where $x_2 = \omega h / v$
 $x_3 = \omega h / c$
 $h = \text{height of burst}$

The result of these calculations show the initial amplitudes are consistent with the data. Figure 7 is a spectral ratio plot of the spherical to plane transmission coefficients. The ratio of the transmission coefficients are greater than 2 for the low frequencies indicating more energy is coupled in the ground through the spherical surface than the plane surface. Attenuation is not a major factor at these low frequencies and ranges. Only a 3% amplitude loss is expected at 25 Hz assuming a Q factor of 10. The average ratio of the first peaks of DFU28 and DFL28 is 2.7, very near to the value in the ratio given in figure 7 for frequencies less than 25 Hz. This brings us to the possibility that there is a definite non-symmetric radiation pattern in the vertical directions with greater energy transmitted through the spherical surface than the plane surface. However, it must be recognized that this is an elastic calculation in areas that have much inelastic behavior.

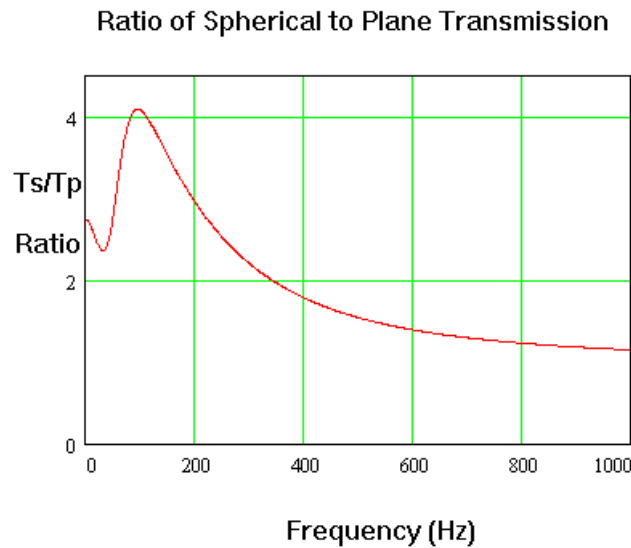


Figure 7

Spectral Ratios of Transmission Coefficients for Plane and Spherical Surfaces

This elastic calculation can be carried out further to approximate the high frequency radial signals directly above or below the source and show it is consistent with the data. Note that in Table I, these signals have peak accelerations of 91.4 G and 17.8 G, a factor of five difference. To account for the

amplitudes analytically, the problem is broken up into three segments in which the wave is transmitted: inside the cavity where the spherical air shock wave exists, the interaction at the medium boundaries and the transmission through the tuff to the gauges. This analysis includes the three mechanisms of energy loss; geometric spreading, interaction at boundary interfaces, and attenuation. Note that attenuation is only included in the transmission through the tuff. To show the consistency of the data, the response below the cavity is used to back out the source function and then propagate the signal to the gauge above the cavity. Assume that the air shock inside the cavity is spherically symmetric and can be represented by a Reduced Displacement Potential (RDP):

$$\Phi_a(\omega) = A_a(\omega)e^{ikr} / r \quad (8)$$

where the symbols are the same as in equation (3) and the subscript refers to the air medium. The displacement is given by equation (4): and is:

$$u_a(\omega) = A_a(\omega) \left\{ \frac{ik}{r} - \frac{1}{r^2} \right\} e^{ikr} \quad (9)$$

where u_a is the displacement in air. This expression is propagated through the spherical surface vertically upward using the transmission coefficient in equation 6, T_s :

$$u = T_s u_a \Big|_{r=q} \quad (10)$$

where q is the radius of the shock front incident to the surface. This expression is propagated further using equation (5). In a similar manner, the path through the plane surface below the source is given as:

$$u = T_p u_a \Big|_{r=h} \quad (11)$$

where h is the height of burst and T_p (equation 7) is the plane surface transmission coefficient. This expression can also be propagated further using equation (5). u_a can be found by using the data at one of the locations (above or below the source) to invert for the air shock wave, i.e., Work the problem backwards assuming u is known. This can be used to calculate the time series at the other location for comparison with the actual signal. In the following example, the signal at DFL28 is used to calculate u_a and generate a response at DFU28 location. Figure 8 is a plot of the radial gauge (DFU28) located directly above the source and a derived signal using data from gauge DFL28 located directly beneath the source. A Q factor of 6 is assumed for attenuation in tuff. Q values of this magnitude are found from data on other tests such as DISTANT ZENITH. Other media properties necessary for the calculation were extracted from site studies such as Containment Evaluation Panel documents or Handbook of Chemistry and Physics⁶. The first peak amplitude fits the data fairly well. There are some obvious differences, but the signals also have definite similarities in peaks and phases. As a crude approximation, the calculation indicates the importance of the boundary surface interface supporting the conclusion that there is a significant non-isotropic radiation pattern emanating from the hemisphere.

Comparison of Radial Signal Above Source
and Signal Generated from Radial Signal
Below source

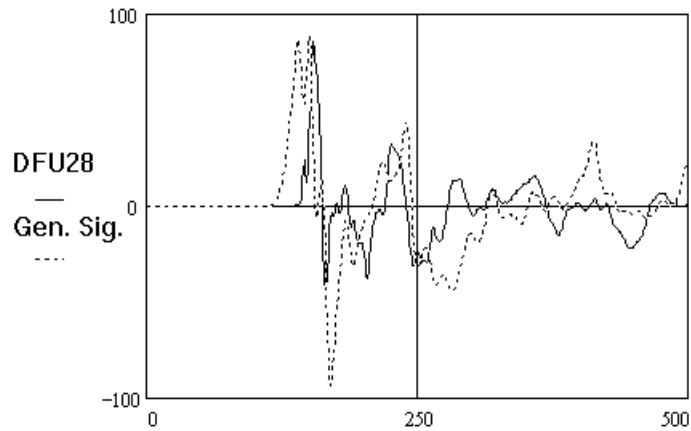


Figure 8

Acceleration (G) Vs Time (Sec)

2) High Frequency Propagation

The high frequency experiment was suggested by our experience with MILL YARD². MILL YARD had free-field triaxial gauges located at ranges of 17 and 24 m. These accelerometers exhibited large high frequency signals compared to tamped explosions. Arrival times indicate that the high frequency signals are a result of the air pressure pulse striking the air-surface interface. Since presently there is no way of distinguishing a cavity source from a tamped source, it is thought that this high frequency signature might discriminate between a tamped and cavity explosion. Thus, the experiment is designed to investigate the behavior of this high frequency signal as it travels to greater ranges. To accomplish this objective, single axis radial accelerometers were placed in 10 m boreholes in the tunnel invert at ranges of 44 m to 224 m in 30 m intervals. The location of the gauges are shown in figure 2. Plots of the signals are given in figures 9 and 10.

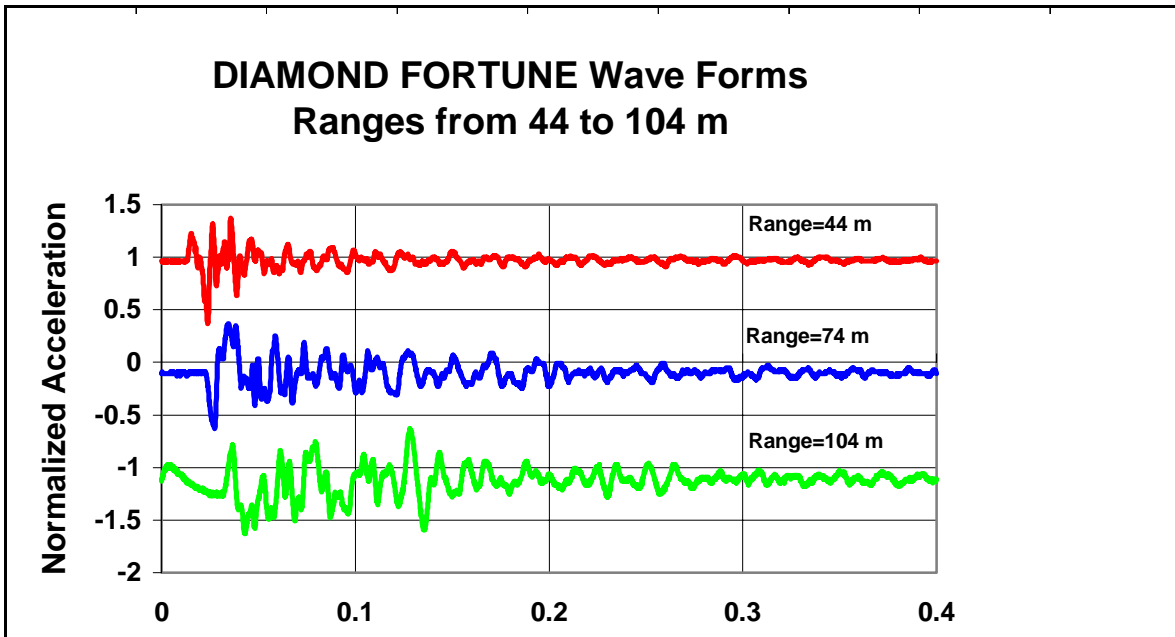


Figure 9

Radial Plots of DIAMOND FORTUNE Signals 44-104 m

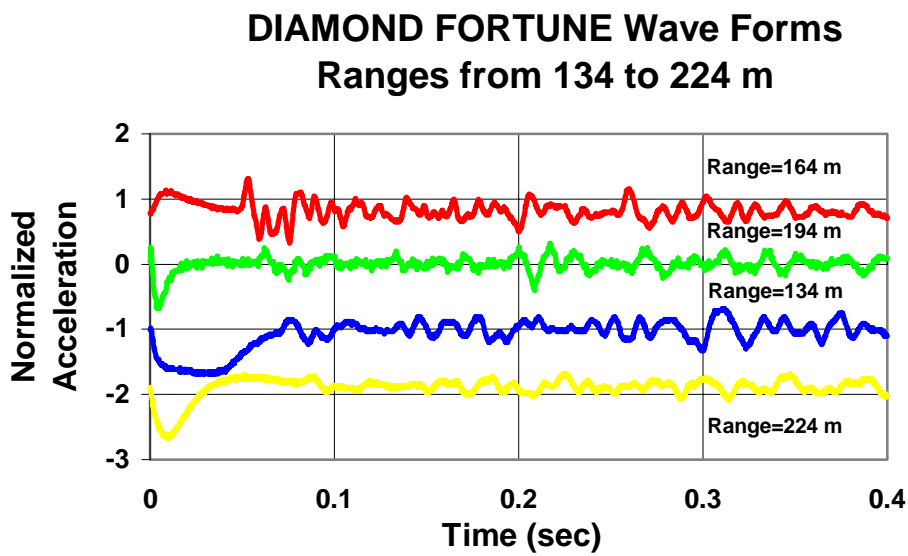


Figure 10

Radial Plots of DIAMOND FORTUNE Signals 134-224 m

There are several things to note on these two figures. The scales are normalized such that the differences between the minimum and maximum for each curve is 1. The plots also have a constant offset artificially introduced so the wave forms don't clutter the figure. The data extends to 0.8 sec. with a sample rate of 10000 samples/sec, but the plot is cut off at 0.4 sec. The signals at ranges of 44 and 74 m look like standard seismic signals with low signal to noise. However, the remaining signals appear to have some type of induced electrical disturbance superimposed at zero time. This is a result of using very conservative estimates of the peak amplitudes prior to the experiment to insure that the data would not clip. This over-estimation of peak amplitude caused the gauges at greater ranges to have signal approaching the noise amplitudes. Thus, the 100 G gauges measured a peak acceleration of 0.04 G at a range of 224 m.

Table of Peak Accelerations

The Low Pass Filter is at 200 hz.

	Range (M)	Peak Acc. (G)	Filtered Peak (G)
DFR44	47.2	2.950	0.84
DFR74	76.2	1.760	0.84
DFR104	100.7	0.490	0.25
DFR134	139.1	0.270	0.17
DFR164	162.8	0.200	0.10
DFR194	195.7	0.054	0.05
DFR224	224.6	0.036	0.02

Table III

Peak Accelerations for Gauges in High Frequency Experiment

Table III is a list of the slant ranges for each gauge with the corresponding acceleration peaks of the first arrivals. One of the columns is the raw data and another is for signals low pass filtered at 200 Hz. The peak accelerations span nearly 2 orders of magnitude over the entire differential range of 180 m. Note that the closest gauge at 44 m has its peak reduced the most by filtering. This is an indication that the high frequencies are being filtered out by attenuation in the earth at greater ranges. Figure 11 is a plot of the spectral amplitudes of three signals for gauges located at the indicated ranges. If a Sharpe⁷ source is assumed, the acceleration spectra should be flat at high frequencies. This is obviously not the case as shown in figure 11. Attenuation causes the spectra to decay significantly at the higher frequencies. Also shown on the plots are the corner frequencies (fc) associated with each spectra. The corner frequencies are found by fitting the low frequencies to an average constant and a log-log straight line to the high frequency decay and noting the intersection. The three spectra in figure 11 also show the trend in which the corner frequencies shift to a lower frequency with increasing range. Also the low frequency Fourier amplitudes decrease with range.

Spectral Amplitudes Radial Gauges

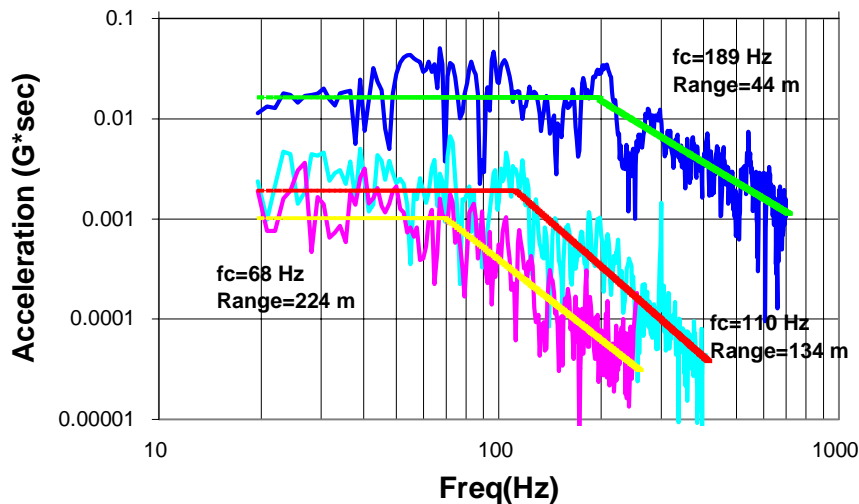


Figure 11

Spectral amplitudes and Corner Frequencies for ground motion
at 3 locations on DIAMOND FORTUNE

The DIAMOND FORTUNE spectra show the high frequency content in the cavity explosion. To contrast this with a tamped explosion, figure 12 shows spectral plots with their corner frequencies of both DIAMOND FORTUNE and DISTANT ZENITH. In this case, DISTANT ZENITH is scaled to the DIAMOND FORTUNE yield. The DIAMOND FORTUNE gauge (DRF44) is at a slant range of 47 m and this particular DISTANCE ZENITH gauge was located at a range of 200 m. The scaling assumes there are 2 orders of magnitude difference between the yields of the two events or a scaling factor near 5. This increased the corner frequency of DISTANT ZENITH from a value near 17 Hz to a scaled frequency of 88 Hz. The range is also scaled from 200 m to 40 m which is nearly equal to the DRF44 range. The plots show that DRF44 has a corner frequency of 189 hz which is over twice the DISTANT ZENITH scaled frequency. There were a total of seven accelerometers sites on DISTANT ZENITH at ranges from 200 to 350 m. The scaled spectrum for each signal was calculated and the range corrected to 44 m. The resulting corner frequencies had an average of 101 Hz which is considerably less than 189 Hz. However, this is not the indicator of a cavity explosion. Figure 12 shows the effects of decoupling quite nicely. The decoupled event has low amplitudes at low frequencies and a higher corner frequency compared to a tamped event. This is just what one would expect if DISTANT ZENITH was a smaller coupled shot.

Spectral Amplitudes of DF and DZ DZ is scaled to DF Yield

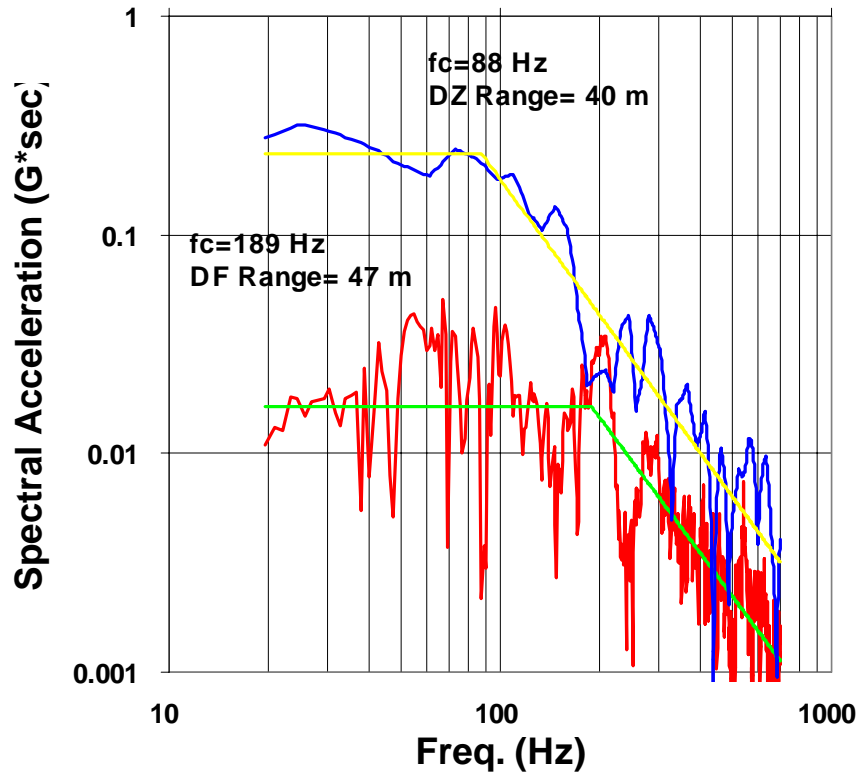


Figure 12

Spectral amplitudes and Corner Frequencies of DISTANT ZENITH (DZ) and DIAMOND FORTUNE (DF)

Table IV is a list of some spectral characteristics of the accelerations in DIAMOND FORTUNE as represented by the examples in figure 11. The table includes data from all the radial gauges in the experiment. The signals above the cavity exhibit very high corner frequencies of 400 and 500 Hz. In general, there is a monotonic decay in corner frequency with range. The slopes of the high frequency spectral decay vary between -1.5 to -3.0, and estimates of Q (Quality Factor) made from these slopes average about 12. The average low frequency offsets also drop-off in a monotonic fashion.

TABLE OF SPECTRAL CHARACTERISTICS OF
DIAMOND FORTUNE

	CORNER FREQUENCY (Hz)	SLOPE	LF OFFSET (G*SEC)
DFU28	397	-2.29	0.12700
DFU22	491	-1.51	0.14800
DFL22	188	-2.08	0.05050
DFL28	176	-2.24	0.06360
DFR44	189	-2.04	0.01630
DFR74	106	-1.69	0.00682
DFR104	123	-2.32	0.00324
DFR134	110	-3.00	0.00192
DFR164	71	-2.50	0.00223
DFR194	71	-2.79	0.00129
DFR224	68	-2.66	0.00102

Table IV

Spectral Characteristics of DIAMOND FORTUNE Signals

Table IV also illustrates differences in the far-field radiation pattern discussed earlier. The low frequency offsets are a measure of the long period transmission (1 Hz) of the source. This portion of the signal should propagate to the far field and be a good indicator of the seismic radiation pattern. Consider the very near-field gauges DFU28, DFU22, DFL28, and DFL22. Note that in Table IV there is a factor of 2.3 between these offsets in DFU28 and DFL28 and 2.6 between DFU22 and DFL22. This feature is consistent with the filtered signals which show a factor of 2 in figure 6 and reinforces the conclusion that the signal is transmitted better through the spherical surface than the plane surface.

3) DIAMOND FORTUNE Decoupling Calculation

Decoupling is estimated in the same manner as MILL YARD² except the ground motion was measured in the free-field as opposed to on the surface. The technique uses spectral amplitude ratios of ground motion from a tamped explosion to the DIAMOND FORTUNE ground motion. DISTANT ZENITH is the reference test and its data is scaled to the same yield and ranges as DIAMOND FORTUNE. This particular event is chosen because it is also in P-Tunnel and occurred less than 1 km from DIAMOND FORTUNE. The ground motion measurements for DISTANT ZENITH were obtained from a linear array of accelerometers extending out radially from the working point (WP) beginning at 200 m to 350 m in 30 m intervals. There are a total of seven 3-component systems of which only the radial signals are used. These are compared to the seven DIAMOND FORTUNE radial gauges at ranges 44 to 224 m. The results of the decoupling analysis are shown in figure 13.

DIAMOND FORTUNE Decoupling DISTANT ZENITH is reference

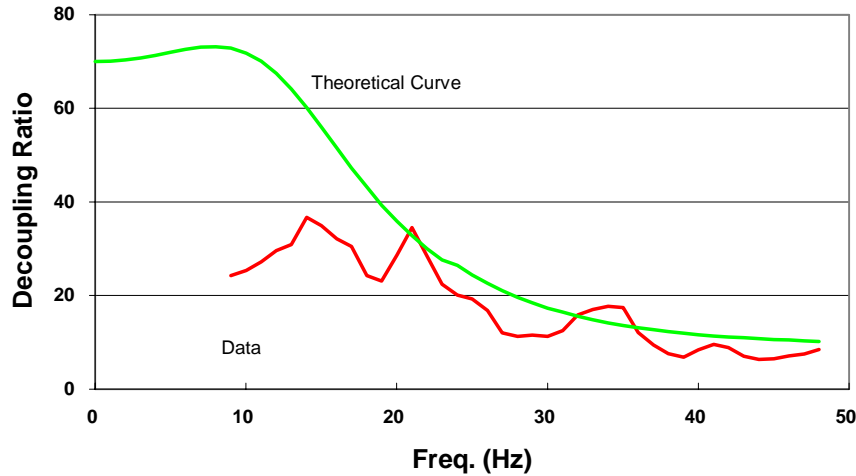


Figure 13

DIAMOND FORTUNE Decoupling

The smooth solid line is a theoretical curve derived from the Sharpe solution⁷ and scaling the elastic radius of the reference event to that of the cavity event. The high frequency decoupling is fixed at 10 and the low frequency decoupling at 70. The value of 10 is chosen because it fits the data at the high frequencies. The 70 is picked because it is near the result in the MILL YARD experiment. The other curve is the decoupling calculated from the average of 49 different pairs of spectral ratio curves. The 49 pairs arise from using the seven DISTANT ZENITH signals as references and comparing with seven DIAMOND FORTUNE signals. Taking all possible permutations of the spectral files gives 49 different spectral ratios. The DISTANT ZENITH reference spectra are calculated by cube root scaling and applying range corrections to match the DIAMOND FORTUNE location. Note that in the low frequency end of the spectrum, the analysis shows much less decoupling than expected. This is probably due to the spurious low frequency electrical signal that was induced into the DIAMOND FORTUNE data (figure 10). Note that decoupling is the ratio of the scaled reference explosion spectrum to the cavity spectrum. If the cavity data is contaminated with low frequency noise effectively increasing the low frequency Fourier amplitudes of DIAMOND FORTUNE, this will lower the decoupling ratio at these frequencies. An attempt was made to remove this noise from the data, but the efforts yield essentially the same results. However, the analysis still shows a large amount of decoupling at 20 Hz. This is more than what was exhibited on MILL YARD² which showed a steep decline in decoupling near 10 Hz and asymptotically approached 10. It is uncertain if the shape of the decoupling curve is due to differences in the height of burst of the devices, or that MILL YARD² decoupling data was calculated using gauges located on the mesa surface whereas DIAMOND FORTUNE used free-field gauges with the signal emanating from the side of the hemisphere.

There is an additional factor that limited the low frequency range of DISTANT ZENITH. The length of the time series recorded on DISTANT ZENITH has considerable impact on the analysis. Notice that the data calculation in figure 13 begins near 9 Hz. The reason for this is the total time recorded for the DISTANT ZENITH experiment was about 1.6 sec. When these data were scaled, the total scaled recorded time is compressed by a factor of 5 (.32 sec). This increases the frequency interval of the FFT by the same factor. A further reduction in the time window is caused by spectral averaging the scaled data. This effectively eliminates the usable low frequency part of the spectrum.

Conclusion:

DIAMOND FORTUNE yielded data for analysis in the three areas of concern: seismic radiation pattern, generation and propagation of high frequency signals and decoupling. The closest gauges in the near field yielded very high quality data. These were accelerometers placed above and below the cavity showing a definite radiation pattern. This is evident not only in the high frequency data, but also in the low frequency filtered signals. The main mechanism appears to be the hemispherical geometry of the cavity with larger signals being transmitted in the direction of the spherical surface when compared to the plane surface. This is consistent with an elastic calculation which indicates that the transmission coefficients of the two boundaries cause propagation through the spherical surface to be over twice as efficient as through the plane surface.

The data at greater ranges are of less quality. This is due to my conservative nature in estimating peak accelerations allowing system noise to be seen on signals at these ranges. Especially troublesome is the unexplained induced electrical noise present on some of the channels. In spite of this, the high frequency results of the MILL YARD event also hold for DIAMOND FORTUNE. The corner frequencies of DIAMOND FORTUNE are twice that of the scaled DISTANT ZENITH. This was hoped that this could be used in the far-field as a way to distinguish tamped explosions from a cavity events. That is, the air shock interaction on the cavity walls would induce more high frequencies than an equivalent tamped explosion. However, this was not apparent in the analysis. The decoupled event look like a coupled event with a lower yield.

DIAMOND FORTUNE was a fully decoupled event. Although the near-field data was contaminated with low frequency noise, the high frequency signals showed decoupling in the range of 10-30. This would imply large decoupling at low frequencies similar to MILL YARD results.

References:

1. M. D. Denny and D. M. Goodman, "A Case Study of the Seismic Source Function: SALMON and STERLING Reevaluated", J. Geophys. Res., 95, 19704-19723, 1990.
2. H. D. Garbin, "Free-field and Decoupling Analysis of MILL YARD Data", SAND86-1702 (Albuquerque, NM:Sandia National Labs, Dec. 1986).
3. W. R. Perret and R. C. Bass, "Free-Field Ground Motion Induced by Underground Explosions", SAND74-0252 (Albuquerque, NM:Sandia National Labs, Feb. 1974).
4. E. P. Chael, "Spectral Discrimination of NTS Explosions and Earthquakes in the Southwestern United States Using High-Frequency Regional Data", Geophys. Res. Lett., 15, 625-628, 1988.
5. D. Bame Carr, "Discrimination Using Spectral Slopes at Frequencies up to 50 Hz", Bull. Seism. Soc. of Amer., 82, 337-351, 1992.
6. R. C. Weast (Editor), "Handbook of Chemistry and Physics", 69 ed. ,The Chemical Rubber Publishing Company, Boca Raton, FL, 1988.
7. J. A. Sharpe, "The Production of Elastic Waves by Explosion Pressures; pt 1: Theory and empirical Field Observations, Geophys. 7, 144-154 (1942).

Distribution:

Lawrence Livermore National Laboratory

Attn: P. Goldstein, L-205
D. B. Harris, L-205
K. K. Nakanishi, L-205
H. J. Patton, L-205
J. Zucca, L-205

Los Alamos National Laboratory

Attn: F. N. App, EES-3, MS F659
W. M. Brunish, EES-3, MS F659
B. W. Stump, EES-3, MS C335
S. R. Taylor, EES-3, MS C335

US Department of Energy Nevada Field Office

Attn: G. C. Allen

P. O. Box 98578

Las Vegas, NV 89193-8518

FC/DSWA, FCTT

W. E. Reinke
B. Ristvet
KAFB, NM 87117

IRIS Data management Center

Attn: Dr. T. Ahern
1408 NE 45th Street
Seattle, WA 98105

USGS

Attn: C. R. Hutt
Albuquerque Seismological Laboratory
KAFB/USGS
Albuquerque, NM 87115-5000

Robert Bass

7705 Cedar Canyon Pl. NE
Albuquerque, NM 87122

MS 0655 5736 P. B. Herrington
MS 0655 5736 D. B. Carr
MS 0655 5736 E. P. Chael
MS 0655 5736 J. P. Claassen
MS 0750 6116 M. C. Walck
MS 0750 6116 G. J. Elbring
MS 0750 6116 C. J. Young
MS 1168 9321 W. B. Boyer
MS 1169 9322 T. K. Bergstresser
MS 1169 9322 C. W. Cook
MS 1169 9322 M. D. Furnish
MS 1169 9322 H. D. Garbin (15)
MS 1159 9311 J. I. Greenwool

MS 1170 9205 P. L. Nelson
MS 1179 9341 R. E. Peppers
MS 1391 9331 M. E. Burke
MS 1391 9331 J. A. Chael
MS 1391 9331 F. M. Raymond
MS 1391 9331 R. C. Shear
MS 9018 8523-2 Central Technical Files
MS 0899 4414 Technical Library (5)
MS 0619 12630 Review & Approval
Desk for DOE/OSTI (2)

